

Experimental and Theoretical Characterization of Multimode Fiber Bragg Grating External Cavity Lasers

Qing-Yang Xu^{*a}, Jian-Wei Mu^b, Chang-Qing Xu^a and Xun Li^b

^a Dept. of Engineering Physics, McMaster Univ., 1280 Main St. W., Hamilton, ON, Canada L8S4L7;

^b Dept. of Electrical and Computer Engineering, McMaster Univ., 1280 Main St. W., Hamilton, ON, Canada L8S4K1

ABSTRACT

In this paper both statistic and dynamic behaviors of the multimode fiber Bragg grating external cavity lasers (MMFBG-ECL) have been studied experimentally, and simulated numerically by time domain traveling wave (TDTW) rate equations. Experimentally, multiple wavelength selection has been realized by offsetting the coupling between the laser diode (LD) and the MMFBG. Small signal modulation responses at these wavelengths have been measured and over 8 GHz modulation bandwidths have been demonstrated at several wavelengths. Numerically, the TDTW model has been employed to simulate the multiple wavelength lasing selection and L-I curves. Comparison between single mode fiber Bragg grating external cavity lasers (SMFBG-ECL) and MMFBG-ECL have been addressed. In addition, steady experiments and numerical simulated are made to verify our numerical model.

Keywords: Multimode fiber Bragg grating, external cavity laser, semiconductor laser, high frequency modulation, time-domain traveling wave equations

1. INTRODUCTION

The rapidly growing demands on the bandwidth of backbone links have made it necessary to increase the transmission capacity in local-area networks (LAN) beyond 1 Gb/s, following various high-speed data networking standards (e.g., Gigabit Ethernet and 10-Gigabit Ethernet). The current installed in-building fiber consists of 62.5/125- μm graded index multimode fibers (GI-MMFs). In order to upgrade the existing MMF links, recently long wavelength (1.3/1.5 μm) wavelength-division-multiplexed local area networks (long wavelength WDM-LANs) have drawn much attention and their communication capacity has been investigated experimentally [1-3, 8]. Long wavelength vertical cavity surface emitting lasers (VCSELs) [2] are ideal light sources for long wavelength WDM-LANs, however, are still under investigation. Multimode fiber Bragg grating external cavity lasers (MMFBG-ECL) [4, 5] are promising devices in such system due to their inherent merits such as low cost, multiple lasing wavelength selection, high output power and compatible with multimode fibers in LAN, as compared with SMFBG-ECLs [6, 7].

High frequency modulation of the MMFBG-ECL has been investigated [4]. However, due to a long external cavity used in the experiments, bad small signal response curve was obtained, which is not nearly enough for high speed modulation. To improve the high frequency response of the device, a short external cavity (4 mm) is employed in this paper. Both statistic and dynamic behaviors of the MMFBG-ECL have been studied. Experimentally, multiple wavelength selection has been realized by offsetting the coupling between the laser diode (LD) and the MMFBG. Small signal modulation responses at the selected wavelengths have been measured and over 8 GHz modulation bandwidths have been demonstrated. Accordingly, system transmission experiment has been carried out over 250 m traditional 62.5 μm core GI-MMF at bit rate of 2.5 Gb/s. On the other hand, time domain traveling wave (TDTW) rate equations [9-12] are used to simulate the performance of the MMFBG-ECL numerically. A set of forward and backward field envelop traveling equations centered at each Bragg wavelength, defined by the Bragg condition of the MMFBG, are implemented to slice the gain curve over the entire gain bandwidth to different sections. Therefore multiple wavelength lasing can be simulated accordingly. Comparison between experiments and numerical simulated are made to verify our numerical model.

*xuq5@mcmaster.ca; phone 1 905 525-9140; fax 1 905 527-8409; www.mcmaster.ca

2. EXPERIMENT RESULTS

2.1 Device structure

Our device is shown schematically in Fig. 1. The device consists of a $1.5\ \mu\text{m}$ single mode ridged FP multiple quantum well (MQW) LD, coupled with a MMFBG imprinted in the standard GIMMF (core diameter of $62.5\text{-}\mu\text{m}$ and numerical aperture (NA) of 0.27) by the UV exposure and phase mask technology. A taper was directly formed on the tip of the MMFBG to enhance the coupling efficiency between the LD and the MMF to up to about 90%. One facet of the LD was antireflection (AR) coated with a residual reflectivity of about 10^{-4} , and the other facet was as cleaved with a reflectivity of 0.32. The MMFBG is 8 mm long and its reflection spectrum is shown in Fig. 2.

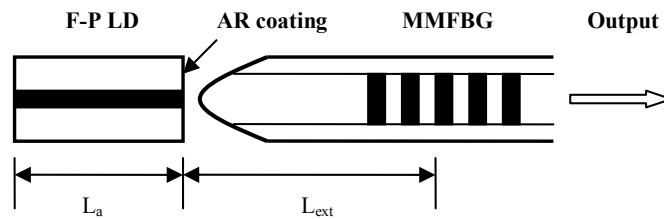


Fig. 1. Schematic structure of the MMFBG-ECL.

2.2 Steady characteristics

The reflection characteristics of the MMFBG were measured, as shown in Fig. 2. It should be noted the reflectivity at each wavelength depends on the excitation situation of different mode groups [4]. In our measurement, the SMF was used to excite the MMFBG, by zero offsetting (i.e., the cores of SMF and MMF are center aligned).

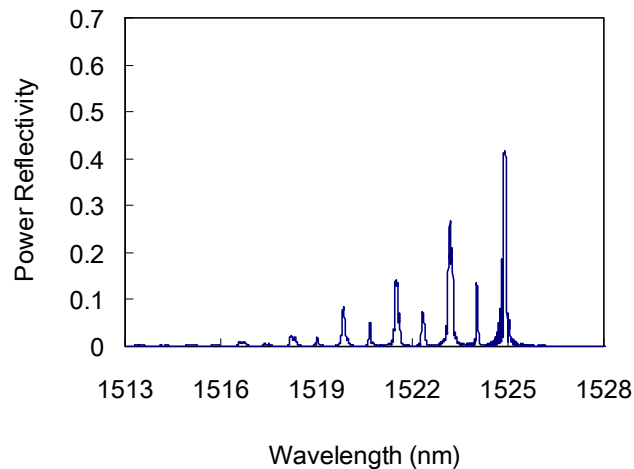


Fig. 2. Reflection spectrum of the MMFBG.

Fig. 3 shows the multiple wavelength lasing by offsetting the coupling between the LD and the MMFBG. Five wavelengths were selected, and the wavelength spacing is around $1.5\ \mu\text{m}$. This wavelength spacing is roughly 100 GHz and therefore facilitates the DWDM channels. Fig. 4 shows optical spectra of five lasing wavelengths by offsetting the coupling between LD and MMFBG. Side mode suppression ratios (SMSR) are larger than 30 dB for all wavelengths.

Fig. 4 is the typical L-I curve for the first 2 wavelengths. The L-I curve of the SMFBG-ECL is also shown for comparison. Threshold currents were 18 and 20 mA, respectively for the two wavelengths of the MMFBG-ECL. In addition, slope efficiencies were both 0.2 W/A. Threshold current was 20 mA and slope efficiency was 0.067 W/A for the SMFBG-ECL. This clearly shows the high output power advantage of the MMFBG-ECL, which will contribute to high signal-to-noise ratio (SNR) than SMFBG-ECL at the same injection current levels.

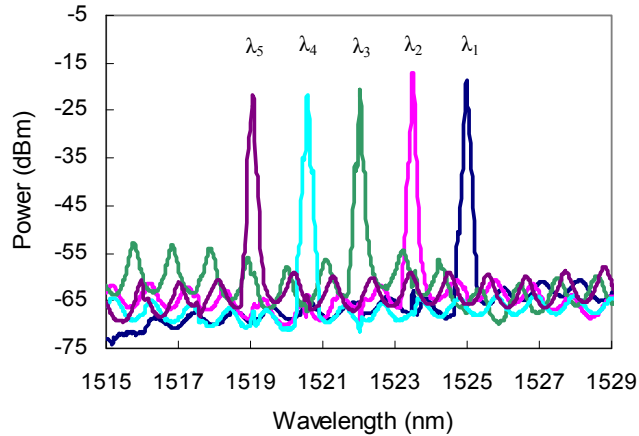


Fig. 3. Optical spectra of five lasing wavelengths by offsetting the coupling between LD and MMFBG.

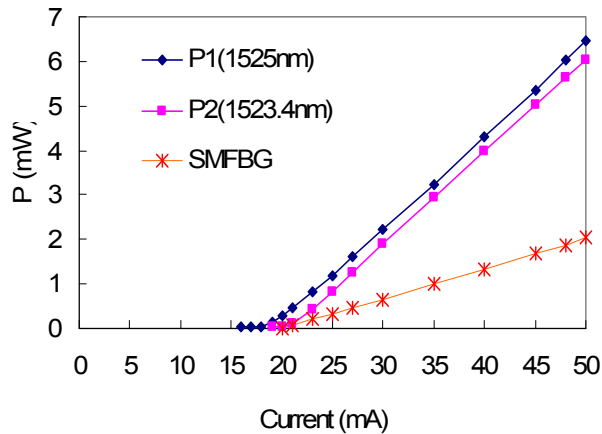


Fig. 4. Measured L-I curves at first two wavelengths of MMFBG-ECL and SMFBG-ECL, respectively.

2.3 Dynamic characteristics measurements

The dynamic characteristics of the MMFBG-ECL were then measured. The small signal response and large signal transmission experiments setup diagram are shown in Fig. 5. A 50 Ω planar waveguide transmission line was used to connect to the microwave measurement equipments. A surface-mounted resistance was attached between to the LD and the transmission line for impedance matching. A bias-T was used to combine the DC current source and the AC modulation signal. Wide-band small-signal frequency responses of λ_1 to λ_5 measured by the Agilent 8703B lightwave component analyzer are shown in Fig. 6. The DC bias current was 40 mA and the RF modulation power from the analyzer was 0 dBm. Due to the reduction of the external cavity length to about 4 mm, the small signal bandwidth of the MMFBG-ECL improves greatly compared to long cavity MMFBG-ECLs [4]. The 3-dB bandwidth at λ_1 , λ_2 , λ_3 and λ_5 were both over 8 GHz.

System transmission experiments were carried out for the designed MMFBG-ECL using the 2.5-Gb/s pseudo-random binary sequence (PRBS) modulation signals. The transmission medium was 250 m GIMMF. An Agilent 83732B synthesized signal generator operated at 2.5 GHz was used to drive the HP70841B pattern generator. The latter generated the 2.5-Gb/s PRBS signals and fed them into the MMFBG-ECL through the planar transmission line. For demonstration purpose, only 2 wavelengths at λ_1 (1525 nm) and λ_2 (1523.5 nm) among those shown in Fig. 3 were selected as optical signal wavelengths in this system demonstration. Light signals were detected by the Agilent 83434A lightwave receiver and measured by the Agilent 86100A wide bandwidth oscilloscope. Eye diagrams at these two different wavelengths

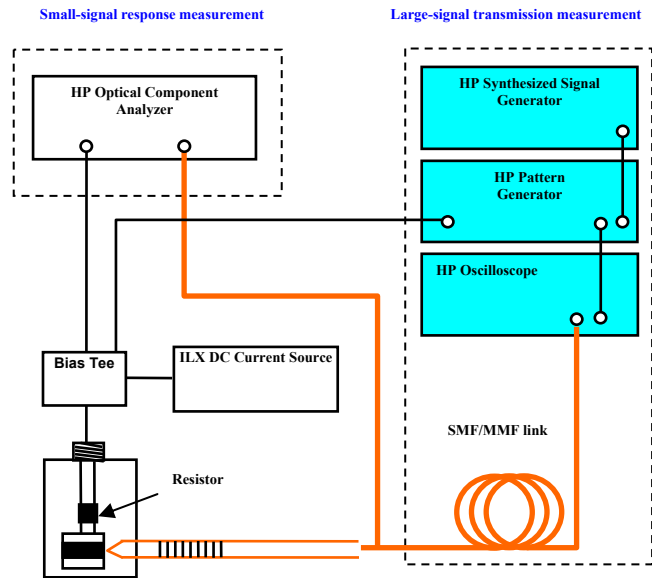


Fig. 5. Small signal response and large signal transmission experiments setup.

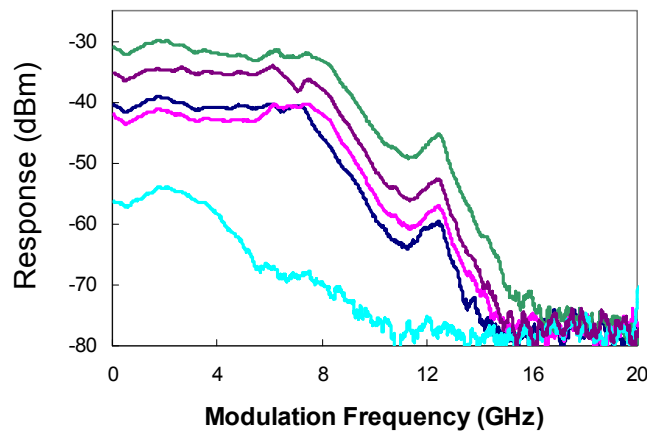


Fig. 6. Small signal response curve for five wavelengths.

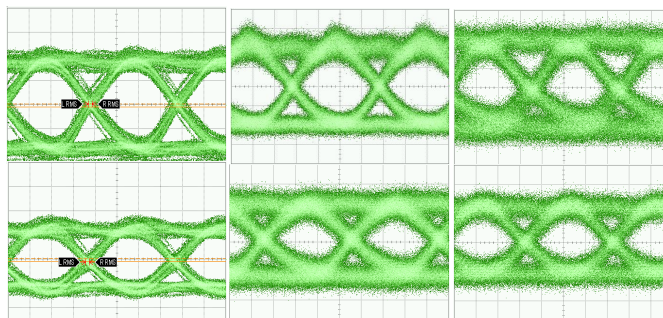


Fig. 7. Eye diagram of the MMFBG-ECL for two different wavelengths (upper row for λ_1 and lower row for λ_2) for back-to-back (left column), over 24 km SMF (middle column) and over 250 m MMF (right column).

(upper row for λ_1 and lower row for λ_2) for back-to-back (left column), over 24 km SMF (middle column) and over 250 m MMF (right column) were recorded by the oscilloscope and are shown in Fig. 3. The eye diagrams proved good transmission performance of our device in the MMF link, as well as long distance transmission performance in the

standard SMF link. This proves the MMFBG-ECL an agile device in different optical communication systems. From Fig. 6, we can expect that even higher transmission speed (>10 Gb/s) is possible, by proper design of the photon resonance enhanced peak in the small signal response curves [7]. (12.5 GHz photon resonance enhanced peaks in our device with 4 mm long external cavity.)

3. NUMERICAL SIMULATION OF THE DEVICE

In this section, time-domain traveling wave (TDTW) rate equations [9-14] were implemented to simulate both the static and dynamic characteristics of the MMFBG-ECL. In order to include the wavelength dependence of the gain curve and reflection curve of the MMFBG, two methods can be used: First, in the wavelength domain the gain curve and the reflection spectrum can be sliced into several sections based on each Bragg reflection center of the MMFBG. Accordingly the gain and reflection spectrum in each wavelength section are both wavelength independent; this means that we can treat each “narrow band” problem by one set TDTW model [9]. As a result, the total wavelength dependant behaviors can be modeled by a set of TDTW equations. The second method is a “wide-band” treatment that considers both the wavelength dependence of the gain curve and the reflection spectrum. With a given gain and reflection curve, a digital filtering technique [14] can be used in the TDTW equations. In this paper the first method is adopted and the second method will be implemented elsewhere.

3.1 Reflection characteristics of a MMFBG

It is well known in the Graded index multimode fiber (GIMMF), the LP modes are highly degenerated such that the propagation constants β_{lm} of the mode group LP_{lm} :

$$\beta_{lm} = k_0 n_{core} \left[1 - \frac{2(2m+l-1)}{k_0 n_{core}} \sqrt{\frac{2\Delta}{a^2}} \right]^{1/2} \quad (1)$$

where a is the core radius of the MMF; k_0 the wave number in vacuum; n_{core} the refractive index of the core; and Δ the maximum relative index difference of the core and cladding. For the GIMMF used in the simulation, parameters are as follows: $a = 31.25 \mu\text{m}$, $\text{N.A.} = 0.27$, $n_{core} = 1.46$.

3.2 Time-domain traveling wave equations

TDTW governing equations for the i th mode group traveling in the cavity are expressed as:

$$\frac{1}{v_g} \frac{\partial F_i(t, z)}{\partial t} + \frac{\partial F_i(t, z)}{\partial z} = \left[\frac{1}{2} (\Gamma g(N, \lambda_i) - \alpha_i) - j\delta_i \right] F_i(t, z) + j\kappa_i R_i(t, z) + s_f \quad (2a)$$

$$\frac{1}{v_g} \frac{\partial R_i(t, z)}{\partial t} - \frac{\partial R_i(t, z)}{\partial z} = \left[\frac{1}{2} (\Gamma g(N, \lambda_i) - \alpha_i) - j\delta_i \right] R_i(t, z) + j\kappa_i F_i(t, z) + s_r \quad (2b)$$

where v_g is the group velocity ($v_g = c/n_g$) of light traveling in the waveguide region, Γ the gain confinement factor, α the waveguide loss caused by scattering and free carrier absorption, κ_i the coupling coefficient between forward and backward fields by the grating in the MMF, and s_f and s_r are the spontaneous noise coupled to forward and backward fields, which are related to the spontaneous emission factor β . s_f and s_r can be simulated by a Gaussian distributed random number generator [12] that satisfies the correlation

$$\langle s(z, t) s^*(z', t') \rangle = \beta K R_{sp} \delta(t - t') \delta(z - z') / v_g \quad (3)$$

where $R_{sp} = \beta N^2 / L$ is the bimolecular recombination per unit length contributed to spontaneous emission, and K is the transverse Petermann factor.

An analytical gain expression for quantum well (QW) materials is used in the simulation. The analytical gain model at these wavelengths for QW materials is

$$g(N, \lambda_i) = a_{Ni} \ln(N / N_{tri}) \quad (4)$$

where a_{Ni} is the differential gain coefficient at wavelength λ_i , and N_{tr} the transparent carrier density.

The associated refractive index changes are also linked to the gain changes analytically through the linewidth enhancement factor (LEF) [12, 13] by

$$n_{eff}(N, \lambda_i) = n_{eff0} + \Delta n(N, \lambda_i) = n_{eff0} - \Gamma \alpha_{mi} g(N, \lambda_i) \quad (5)$$

The detuning factor δ_i of the MMFBG is the reference wavelength deviation from the Bragg condition, which is defined as

$$\delta_i(N, \lambda_i) = \frac{\omega_i}{c} n_{effi} - \frac{\pi}{\Lambda} \quad (6)$$

where n_{effi} is the effective refractive index of each mode group, and Λ the Bragg wavelength of the grating, which is defined by $\lambda_i = 2n_{effi}\Lambda$.

Simultaneously, the time dependent carrier density rate equation in the active region is given by

$$\frac{dN(z,t)}{dt} = \frac{J(z,t)}{ed} - AN(z,t) - BN^2(z,t) - CN^3(z,t) - \Gamma v_g \sum_i g(N, \lambda_i) S_i(z,t) \quad (7a)$$

where $J(z, t)$ is injected current density in the active region, e the electron charge, and d the active waveguide thickness.

The photon densities are expressed in terms of forward and backward field

$$\sum_i S_i(z,t) = \sum_i |F_i(z,t) + R_i(z,t)|^2 \quad (7b)$$

Boundary conditions at $z = 0$ and $z = L$ are given by

$$\begin{aligned} F_i(t,0) &= r_L R_i(t,0) \\ R_i(t,L) &= r_R F_i(t,L) \end{aligned} \quad (8)$$

where r_L and r_R are the reflectivity of the left facet of the LD and right facet of the MMFBG, respectively. Table 1 is the LD parameters used in the simulation.

LD parameters [9, 12]	
SRH and surface recombination reate (A)	$2.8 \times 10^8 \text{ s}^{-1}$
Bimolecular recombination coefficient (B)	$1 \times 10^{-10} \text{ cm}^3 \text{ s}^{-1}$
Auger recombination coefficient (C)	$1 \times 10^{-29} \text{ cm}^6 \text{ s}^{-1}$
Absorption and scattering loss (a)	10 cm^{-1}
Effective phase refractive index (n_{eff})	3.28
Effective group refractive index (n_g)	3.7
Wave guide confinement factor (Γ)	0.05
Length of the LD section (L_1)	400 μm
LD facet residual reflectivity	10^{-4}
Width of the active layer (W)	3 μm
Thickness of the active layer (d)	0.18 μm
Spontaneous coupling factor (β)	10^{-4}
Nonlinear gain suppression coefficient (ϵ)	$3 \times 10^{-17} \text{ cm}^3$

Table 1. LD parameters used in the simulation.

To calculate the coupling efficiency between the LD and different LP mode groups, the overlap integrals for the mode profiles were used

$$\eta_{lm} = \frac{\left| \iint \psi_l^* \psi_{lm} dS \right|}{\sqrt{\iint |\psi_l|^2 dS \cdot \iint |\psi_{lm}|^2 dS}} \quad (9)$$

where ψ_l is the LD mode profile and ψ_{lm} the mode profile of the (l, m) LP mode groups.

3.3 Steady characteristics simulation

In this section, the steady characteristics of the MMFBG-ECL were simulated. Fig. 8 shows L-I curve of the MMFBG-ECL at first two wavelengths. Threshold currents were 18 and 20 mA, respectively. Slope efficiencies were 0.21 and 0.2 W/A, respectively. Again for comparison, SMFBG-ECL was simulated simultaneously. Threshold current was 20 mA and slope efficiency was 0.067 W/A. This fits the experimental results (Fig. 4) quite well. Fig. 9 shows the simulated optical spectra at these two wavelengths. It can be seen from the figure that the TDTW model is quite straightforward to simulate the spectral property of the device.

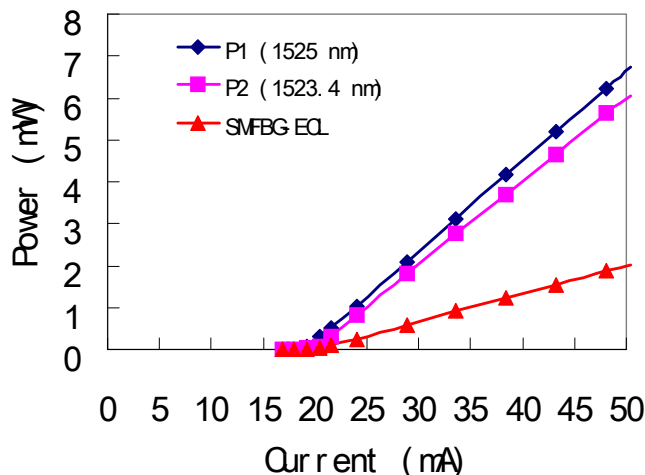


Fig. 8. Simulated L-I curve at first two wavelengths of the MMFBG-ECL and SMFBG-ECL, respectively.

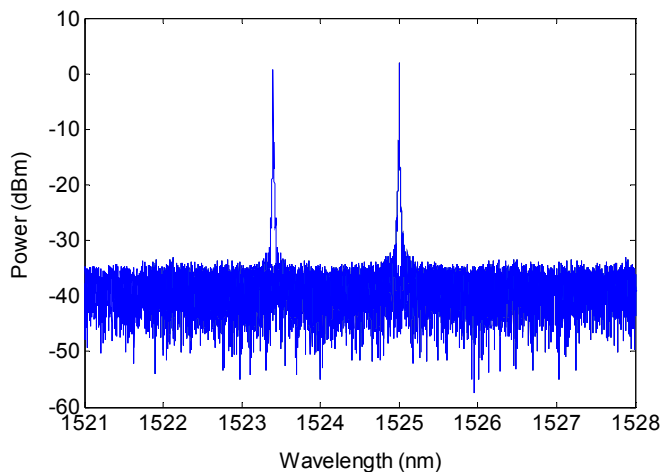


Fig. 9. Optical spectra at first two wavelengths of the MMFBG-ECL.

4. CONCLUSION

In this paper, statistic and dynamic behaviors of the MMFBG-ECL have been studied experimentally. Compared with SMFBG-ECL, MMFBG-ECL have shown promising properties such as multiple wavelength selection, high output power, and high speed modulation at each wavelength, which facilitate long wavelength WDM-LAN requirements. System transmission experiments over 250 m GIMMF have been demonstrated the excellent transmission performance of MMFBG-ECLs. On the other hand, the steady characteristics such as the multiple wavelength lasing and L-I curves have been simulated numerically by TDTW rate equations. Lasing at two wavelengths has been simulated and fits experiments results quite well. Dynamic behaviors simulation will be done in future work.

REFERENCES

- [1] Ramana Murty, M. V., Huang, X. D., Liu, G. L., Lin, C. C., Xu, D., Shieh, C. L., Lee, H. C. and Cheng, Julian, "Long-wavelength VCSEL-based CWDM scheme for 10-GbE links," *IEEE Photon. Technol. Lett.*, vol. 17, no. 6, 1286–1288 (2005).
- [2] Gasulla, I. and Capmany, J., "1 Tb/s·km multimode fiber link combining WDM transmission and low-linewidth lasers," *Opt. Express*, vol. 16, no. 11, 8033–8038 (2008).
- [3] Gu, X. J., Mohammed, W. and Smith, P. W., "Demonstration of all-fiber WDM for multimode fiber local area networks," *IEEE Photon. Technol. Lett.*, vol. 18, no. 1, 244–246 (2006).
- [4] Yu, H.-G., Wang, Y., Xu, C.-Q. and Vandermeer, A. D., "Oscillation wavelength selection of semiconductor lasers using a multimode fiber Bragg grating," *Opt. Express*, vol. 13, no. 5, 1660–1665 (2005).
- [5] Yu, H.-G., Wang, Y., Xu, Q.-Y. and Xu, C.-Q., "Characteristics of multimode fiber Bragg gratings and their influences on external-cavity semiconductor lasers," *IEEE J. Lightwave Technol.*, vol. 24, no. 4, 1903–1912 (2006).
- [6] Hashimoto, J. -I., Takagi, T., Kato, T., Sasaki, G., Shigehara, M., Murashima, K., Shiozaki, M. and Iwashima, T., "Fiber-Bragg-Grating External Cavity Semiconductor Laser (FGL) Module for DWDM Transmission," *IEEE J. Lightwave Technol.*, vol. 21, no. 9, 2002–2009 (2003).
- [7] Paoletti, R., Meliga, M., Rossi, G., Scofet, M. and Tallone, L., "15-GHz modulation bandwidth, ultralow-chirp 1.55- μ m directly modulated hybrid distributed Bragg reflector (HDBR) laser source," *IEEE Photon. Technol. Lett.*, vol. 10, no. 2, 1691–1693 (1998).
- [8] Tyler, E. J., Kourtessis, P., Webster, M., Rochart, E., Quinlan, T., Dudley, S. E. M., Walker, S. D., Pentz, R. V. and White, I. H., "Toward terabit-per-second capacities over multimode fiber links using SCM/WDM techniques," *J. Lightwave Technol.*, Vol. 21, no. 12, 3237–3243, (2003).
- [9] Xu, Q., Hong, X., Liang, W., Li, X., Xu, C.-Q. and Huang, W.-P., "Simulation of crosstalk in integrated distributed feedback laser-photodiode optical transceivers," in *Proc. SPIE*, vol. 6343I, 63431D1-9, (2006).
- [10] Hong, X., Xu, Q., Liang, W., Huang, W.-P., Li, X. and Xu, C.-Q., "Crosstalk analysis in in-line transceiver," in *Proc. SPIE*, vol. 6796, pp. 67963I, (2007).
- [11] Li, X., Sadvnikov, A. D., Huang, W.-P. and Makino, T., "A physics-based three-dimensional model for distributed feedback laser diodes," *IEEE J. Quantum Electron.*, vol. 34, no.9, pp. 1545-1553, Sep. 1998:
- [12] Zhang, L. M., Yu, S. F., Nowell, M. C., Marcenac, D. D., Carroll, J. E. and Plumb, R. G. S., "Dynamic analysis of radiation and side-mode suppression in a second-order DFB laser using time-domain large-signal traveling wave model," *IEEE J. Quantum Electron.*, vol. 30, pp. 1389-1395, Jun. 1994.
- [13] Kim, B. S., Chung, Y. and Lee, J. S., "An efficient split-step time-domain dynamic modeling of DFB/DBR laser diodes," *IEEE J. Quantum Electron.*, vol. 36, 787-794 (1999).
- [14] Li, W., Huang, W.-P. and Li, X., "Digital filter approach for simulation of a complex integrated laser diode based on the traveling-wave model," *IEEE J. Quantum Electron.*, vol. 40, no. 5, 473–480 (2004).